Removal of Hexavalent Chromium from Aqueous Solution using Unmodified saw Dust: Batch and Column Studies

Original research paper

Abstract

The effects of contact time at three initial concentrations and temperature in batch process and the effects of three initial concentrations and three bed heights in column process were used to evaluate the potentials of unmodified saw dust, a low cost adsorbent in removing Cr(VI) with highly mutagenic and carcinogenic properties from aqueous solution. The material characterized using point of zero charge, FTIR and Scanning Electron Microscopy (SEM) showed that it has good adsorbent properties. Nearly 99 % of Cr(VI) was removed in two minutes attaining equilibrium in five minutes for all the initial concentrations tested in batch operation. Langmuir and Dubinin-Radushkevich (D-R) isotherms best fitted the adsorption with maximum adsorption capacities of over 196 mg/g. Adsorption on unmodified saw dust can be physical, ion exchange and chemical depending on the initial concentration and the process is spontaneous and endothermic. The removal efficiency increases with increasing bed height but decreases with increase initial concentration, however, adsorption capacity increases with increase in initial concentration but decreases with increase bed height for column operation. Thomas kinetic model best described the column adsorption over other tested model. Unmodified saw dust can effectively remove Cr(VI) from wastewater in batch and column operations.

Keywords: Adsorption; Hexavalent chromium; Saw dust; Wastewater; Batch; Column.

1. INTRODUCTION

Environmental pollution resulting from solid waste generated from the tannery industry and steel industries are receiving scientific attention worldwide primarily because of their chromium presence [1, 2]. This is due to its mutagenic and carcinogenic properties. Chrome tanning is used for nearly 90 % of the leather produced globally [3]. The spent chrome liquor may contain chromium (III) up to the extent of 2900-5400 mg/L [4]. Chromium enters natural waters by weathering of chromium-containing rocks, direct discharge from industrial operations, wet and dry deposition, and leaching from soils. These aqueous environments do contain oxidizing agents, such as MnO_2 and Mn^{+3} in sufficiently high concentrations to produce measurable yields of chromium (VI) from Cr(III).

Dissolved oxygen by itself does not caused significant oxidation of chromium (III) [5]. The most common and stable forms of chromium in nature are Cr(III) and Cr(VI), though it exists in other oxidation states. While trivalent chromium in trace amounts is considered essential for human health, Cr(VI) has no known usefulness and is a known carcinogen and is harmful for human health [2]. Chromium (III) is seldom found in potable waters while chromium (VI) is often found in waters and is a notorious environmental pollutant because it is a strong oxidant ~~(Bruce, 2002)~~ [6]. The half-life and bioavailability of Cr(VI) in humans is 39 hours and 6.9 % respectively against a half-life of 10 hours and bioavailability of 0.13 % for Cr(III) [2]. Beside its carcinogenic effects, Cr(VI) also cause strong allergic reactions, several effects on the respiratory tract and complications during pregnancy and childbirth [2]. Though WHO recommends 0.05 mg/L of Cr(VI) in drinking water [7], other international organizations and countries have equally developed other standards to cope with chromium toxicity [2].

Like other heavy metals, several methods have been employed to remove Cr(VI) from wastewater and drinking water to meet regulated standards [8]. However, these methods are limited by high operational costs, low levels of pollutants removal, requiring high energy and further disposal cost or treatment of the resulting sludge. Of these methods, adsorption is more preferable especially in developing countries because it cheap with low energy requirements, easy to operate, removes very low levels of organic and inorganic pollutants. Added to these advantages, is the possibility of using very cheap and available low-cost waste materials as adsorbents in replacement of activated carbon which has been found to be the most widely used adsorbent. But its high cost of production and generation of further sludge puts some constraints on its application [9]. Thus, cheap and effective adsorbents have been developed from plant-derived biomaterials such as coconut husk, orange peel, wheat bran, meranti saw dust and spent tea leaves [10]; castor tree leaves, palm trees, peanut shell, lotus leaf, Americana fibers, agave peanut husk and hyacinth leaves [11].

The processing of wood using operations such as sawing, milling, routing, drilling and sanding at saw mills generate huge quantities of solid wastes and by products called saw dust. It is rich in lignin and cellulose which contain many functional groups such as hydroxyl groups, carboxylate and ether groups which can serve as binding sites for chromium. There has been an increased interest in the use of sawdust for adsorption because of significant results that have been reported by various studies [10]. This work therefore studied the efficiency of unmodified saw dust in adsorbing Cr(VI) from aqueous solution. Adsorption data from the effects of contact time at three initial concentrations and temperature studied were used to perform isotherm, kinetics and thermodynamic analyses to calculate

batch adsorption process parameters. Meanwhile, the effects of initial concentration and bed height were studied in column process and the results modeled with Thomas and Young-Nelson kinetic models. Results of this study will contribute in the valorization of agricultural/plant waste materials and enhance cheaper water treatment technics.

2. MATERIALS AND METHODS

2.1. Unmodified Saw Dust Sampling and Characterization

The saw dust used for this study was collected at the plank saw mill located in Comice neighbourhood of Maroua (N $10^0$35.702‘ E $14^0$18.640’). The saw dust collected resulted from a mixture of different types of woods. Soil and other impurities were removed from the saw dust by washing several times with distilled water, followed by filtration on Whitman filter paper N^o 1 and drying for 14 days at laboratory temperature (≈35^{o}C). The dried sample was then sieved to obtain particles <0.5mm which were stored in polyethylene bottles for characterization and adsorption studies.

Surface charge indicated by point of zero charge (PZC) and acidity or basicity of the adsorbent's surface was determined as described by [12] with modifications. Five suspensions each containing 50 mL of NaCl (0.01M) and 0.1 g of sorbent were prepared. These suspensions starting pH (2, 4, 6, 8, and10) were fixed by using NaOH (0.1M) or HCl (0.1M) solutions. The five suspensions were each stirred for 60 minutes and allowed to stand for 48 hours during which the final pH of the suspensions were measured, and ΔpH was calculated as the difference between initial and final pH. For determination of the acidity or basicity of the adsorbent's surface, 0.1 g of dry adsorbent sample was added to 50 mL of distilled water and stirred for 60 minutes. The suspension was kept for 48 hours at the room temperature to reach equilibrium, and then the final pH was measured.

Fourier transform infrared spectroscopy (FTIR, iS50 RAMAN) was used to determine the functional groups, while the morphology and porosity was determined using scanning electron microscopy (FEI QUANTA 200 SEM).

2.2. Procedure of Batch Experiments

A 1000 mg/L stock solution of Cr(VI) was prepared as described by [13], in which 2.829 g of potassium dichromate ($K_2Cr_2O_7$) was dissolved in 1 liter of distilled water. Analytical grade chemicals and reagents were used throughout the study. The stock solution was then diluted with distilled water to obtain Cr(VI) working solutions. 250-mL stoppered Erlenmeyer flasks containing 100 mL of working solution were used to carry out all batch experiments. The dependence of adsorption on contact time

was studied (0-20 minutes) with three initial concentrations (10, 50 and 100 mg/L) using a fixed adsorbent dosage of 0.05 g for each concentration. Equally, the effect of Cr(VI) solution temperature (25- 60^{o}C) on the adsorption process at 100 mg/L initial Cr(VI) concentration and 0.05 g of adsorbent at each temperature was also studied. In each case, the flask with its content was shaken at 150 rpm and Cr(VI) solutions withdrawn at regular time intervals and filtered on a Whatman filter paper N^{0} 1. The Cr(VI) concentration not adsorbed was determined using 1,5 diphenylcarbazyde method [13] on a UV/visible spectrophotometer (spectro 23RS, labo med.inc) at 540 nm and amounts in mg/g and percentage adsorbed calculated by relevant equations [14].

2.3. Batch Adsorption Kinetics Modeling

Data obtained from the study of the effect of contact in this work was tested with Pseudo-first-order, pseudo-second-order and intraparticle diffusion models [14].

The pseudo-first-order kinetic model in its linearized form is given by the Lagergren equation [15]:

$$\ln(q_e - q_t) = \ln q_e - k_1 t \qquad (3)$$

Where q_t is adsorption (mg/g) at time t (min), q_e, is the equilibrium adsorption capacity (mg/g) and K_1 is the pseudo-first-order equilibrium rate constant (min^{-1}) determined from a plot of $\ln(q_e - q_t)$ versus t.

The pseudo-second-order kinetic model expression is described by Ho's linearized equation [15]:

$$\frac{t}{q_t} = \frac{1}{k_2 q_e^2} + \frac{t}{q_e} \quad \text{or} \quad \frac{t}{q_t} = \frac{1}{h} + \frac{t}{q_e} \qquad (4)$$

The initial adsorption rate, h (mg/g·min), as t → 0 can be defined as $h = k_2 qe^2$. The initial adsorption rate (h), the equilibrium adsorption capacity (q_e), and the second-order constant (k_2) can be determined experimentally from the slope and intercept of plot t/qt versus t.

The intra-particle diffusion equation is given as [15]:

$$q_t = k_{id} t^{1/2} + C \qquad (5)$$

Where q_t (mg g^{-1}) is the amount adsorbed at time t (min), k_{id} (mg g^{-1} $min^{1/2}$) is the rate constant of intra-particle diffusion and C is intercept obtained from a straight line plot of q_t versus $t^{1/2}$.

2.4. Batch Equilibrium Adsorption Isotherms

Equilibrium adsorption isotherms are used in the determination of adsorption capacity and the nature of adsorbate-adsorbent interactions [16]. Sorption equilibrium data obtained from study of the effect of contact in this work was tested with Langmuir, Freundlich and Dubinin–Radushkevich (D–R) isotherms.

The Langmuir isotherm is meant for monolayer adsorption taking place over an even homogeneous adsorbent surface [11]. The linearized form of this model is given by:

$$\frac{C_e}{q_e} = \frac{1}{bq_m} + \left(\frac{1}{q_m}\right) C_e \qquad (6)$$

Where C_e is equilibrium concentration of the ionic species (mg/L), q_e is the equilibrium adsorption capacity (mg/g), q_m represents the monolayer adsorption capacity (mg/g), and b is the Langmuir isotherm constant (L/mg). Separation factor, R_L, which is considered as a more reliable indicator of the adsorption is defined by the equation:

$$R_L = \frac{1}{1+bC_0} \qquad (7)$$

Where, b (L/mg) is the Langmuir constant and C_0 (mg/L) the initial concentration of solute. For favorable adsorption, $0 < R_L < 1$; while $R_L > 1$, $R_L = 1$ and $R_L = 0$, respectively, describe unfavorable, linear and irreversible adsorption [11].

The Freundlich model describes multilayer adsorption process which takes place on heterogeneous surface [11]. Freundlich isotherm model can be written as according the formula:

$$q_e = K_F C_e^{1/n} \qquad (8)$$

and the linearized from given by:

$$\ln q_e = \ln K_F + \frac{1}{n} \ln C_e \qquad (9)$$

Where K_F is the Freundlich constant (mg/g)(L/mg)$^{1/n}$ and n is the Freundlich exponent (dimensionless) which defines intensity of the adsorption process.

The Dubinin–Radushkevich (D–R) isotherm [17], which assumes a heterogeneous surface, is expressed as follows:

$q_e = X_m \exp(-K\varepsilon^2)$ (10)

where ε (the Polanyi potential) = $RT \ln(1 + 1/C_e)$, q_e is the amount adsorbed per unit weight of adsorbent (mg g^{-1}), Xm the adsorption capacity of the sorbent (mg g^{-1}), C_e the equilibrium concentration in solution (mg L^{-1}), K is a constant related to the adsorption energy (mol^2 kJ^{-2}), R the gas constant (kJ K^{-1} mol^{-1}), and T is the temperature (K). Plot of $\ln q_e$ versus ε^2 gives X_m and K values. The significance of applying D–R model is to determine apparent adsorption energy, E (kJ/mol) which is given by:

$E = 1/\sqrt{2K}$ (11)

2.5. Evaluation of Batch Adsorption Thermodynamic Parameters

Thermodynamics parameters such as Gibbs free energy (ΔG), enthalpy (ΔH), and entropy (ΔS) are vital for proper assessment of any adsorption process [18]. The experimental data for the effect of temperature on Cr(VI) adsorption on unmodified saw dust was used to calculate the thermodynamic properties by employing the following equations;

$\Delta G = -RT\ln K$ (12)

$\ln K = (\Delta S/R) - (\Delta H/RT)$ (13)

Where R is the ideal gas constant (kJ mol^{-1} K^{-1}) and T is the temperature (K). The enthalpy change (ΔH) and the entropy change (ΔS) are calculated from a plot of lnK versus 1/T.

K is calculated from $K = C_{ads}/C_e$ (14)

$C_{ads} = C_o - C_e$

Where K is the equilibrium constant, C_e is equilibrium (mg/L) at temperature T, C_o is the initial Cr(VI)concentration (mg/L), C_{ads} is the concentration of Cr(VI) in the adsorbent at equilibrium (mg/L) at temperature T.

2.6. Column Adsorption Experiments

Continuous flow adsorption experiments were conducted in glass columns of 2.5 cm inside diameter and height of 30 cm.

The column was filled with the adsorbent between two graded levels of sand (5cm of sand with particles > 250 µm and less than 315 µm from the bottom and 3 cm of large grain size from the top) to avoid loss of adsorbent and also to ensure a closely packed column. Prior to adsorption, a series of distilled water filtration were done in the column in order to eliminate air bubbles inside the column. Two parameters; initial concentration (5, 10 and 50 mg/L) and bed height (3.5, 7 and 10 cm) were studied in the column tests. At the top of the column, the influent Cr(VI) solution was led into the packed column at flow rate 17.28 mL/min, using an adapted high-density polyethylene drip bag. Samples were collected from the exit of the column at regular time intervals and analyzed for residual Cr(VI) concentration.

2.6.1. Column Data Analysis

Column adsorption characteristics were studied by analyzing the shape of the experimental breakthrough curves. They are usually expressed in terms of adsorbed concentration (C_{ad}), inlet concentration (C_o), outlet concentration (C_t), or normalized concentration, defined as the ratio of outlet concentration to the inlet concentration (C_t/C_o), as a function of time or volume of effluent for a given bed height [19]. The exhaust point is determined when C_t changes to 95 % of C_o [20]. The effluent volume (V_{eff}) can be calculated as:

$$V_{eff} = Qt_{total} \qquad (15)$$

Where, V_{eff} is the effluent volume collected (mL); Q is the volumetric flow rate (mL/min), and t_{total} is the total flow time (min). The total amount adsorbed for a given flow rate, feed concentration, and bed height is given by the equation:

$$q_{total} = \frac{QA}{1000} = \frac{Q}{1000}\int_{t=0}^{t=t_{total}} C_{ad}\,dt \qquad (16)$$

Where q_{total} is the maximum column capacity (mg); Q is the inlet flow rate (mL/min); C_{ad} is adsorbed dye concentration (mg/L). The area under the breakthrough curve (A) is obtained by integrating the adsorbed concentration (Cad in mg/L) versus t (min). This area was obtained using Origin 8 software.

The equilibrium metal uptake q_{eq}, or the maximum capacity of the column is defined as the total amount of metal sorbed (q_{total}) per g of adsorbent (W) at the end of the total flow time and can be calculated as:

$$q_{exp} = \frac{q_{total}}{W} \qquad (17)$$

Where q_{total} is the amount adsorbed (mg) and W is the weight of adsorbent (g). The total amount of adsorbate that enters the column is given by the following equation:

$$M_{total} = \frac{C_o Q t_{total}}{1000} \qquad (18)$$

Where M_{total} is the total amount of Cr(VI) ions dispatched to the column (mg); C_o is the initial Cr(VI) concentration (mg/L); Q is the volumetric flow rate (mL/min); and t_{total} is the total flow time (min).

The total percentage removal of Cr(VI) is given by:

$$\text{Total \% Removal} = \frac{q_{total}}{M_{total}} \times 100 \qquad (19)$$

2.6.2. Column Dynamic Adsorption Modeling

Different mathematical models can be used to describe the column behavior. Thomas and Yoon-Nelson models have been used in analyzing the kinetics of adsorption in a column [20]. Thus, these two models were tested in this study to find the best model defining the adsorption kinetics, evaluate the breakthrough performance and determine the adsorption capacity of the column.

Thomas model is based on the mass transfer model which postulates that adsorbate emigrates from the solution to a film around the particle and expands through the liquid film to the surface of the adsorbent. Subsequently, this step is followed by intraparticle diffusion and adsorption on the active site. Its assume Langmuir isotherm for equilibrium, plug flow performance in the bed and second-order reversible reaction kinetics [20, 21]. The linear form of the Thomas model is expressed by the

$$\ln\left(\frac{C_o}{C_t} - 1\right) = \frac{K_{Th} q_o W}{Q} - K_{Th} C_o t \qquad (20)$$

where k_{Th} (ml/min mg) is the Thomas rate constant; q_0 (mg/g) the equilibrium Cr(VI) uptake per g of the adsorbent; Co (mg/L) the inlet Cr(VI) concentration; C_t (mg/L) the outlet concentration at time t; W (g) the mass of adsorbent; Q (mL/min) the flow rate; and t (min) the flow time. The value of K_{TH} and q_o are determined from the slope and intercept of a plot of ln (Co/Ct – 1) versus t.

The Yoon-Nelson model is based on the assumption that the rate of decrease in the probability of adsorption for each adsorbate molecule is proportional to the probability of adsorbate adsorption and the probability of adsorption breakthrough on the adsorbent. The linear form of Yoon-Nelson model is given by the equation:

$$\ln\left(\frac{C_t}{C_o - C_t}\right) = K_{YN}t - K_{YN}\tau \quad (21)$$

Where k_{YN} (min^{-1}) is the Yoon-Nelson proportionality constant and τ (min) the time required for 50 % breakthrough (min). The values K_{YN} and τ are determined from the slope and intercept of $\ln(C_t/C_o-C_t)$ versus t.

3. RESULTS AND DISCUSSION

3.1. Characterization of Adsorbent

For the determination of the point of zero charge, the initial pH of the Cr(VI) solution was plotted against ΔpH(the difference between the initial (pH_i) and final (pH_f) pH values of solutions). The point of intersection of the plot at ΔpH=0 is the point of zero charge (PZC) (Fig. 1) in which the surface acquires a net zero charge. The value of 2.2 was obtained for unmodified saw dust (Fig. 1). Point of zero charge is a pH value at which the sum of negative charges equals the sum of positive charges and the net charge on the surface is zero. Thus, the surface of unmodified saw dust is positively charged at Cr(VI) solution pH values below 2.2 and negatively charged at Cr(VI) solution pH greater than 2.2 [12]. From the acidity and basicity determination, the pH of unmodified saw dust was found to be 8.29 indicating it is a negatively charged material hence favourable for cationic adsorption.

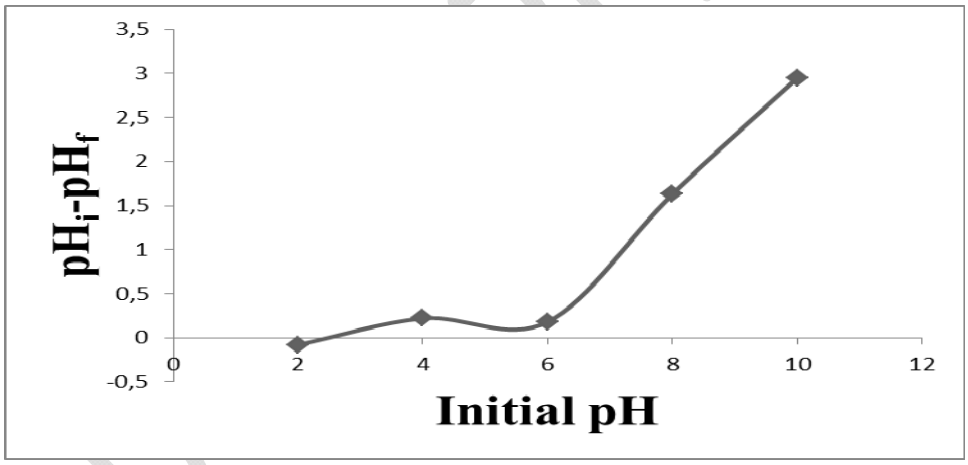

Fig. 1. PZC of unmodified saw dust

The FT-IR spectrum of the unmodified sawdust is shown in Fig. 2. Several peaks are shown by this spectra indicating that unmodified saw dust is composed of various functional groups which can be

used to bind Cr(VI) molecules. The peaks occurring at 3338.14 cm^{-1} and 2916.51 cm^{-1} represents O-H bond of aromatic and aliphatic phenol structures of lignin and cellulose and the asymmetric elongation of the C-H bond of the cellulose respectively [4]. The peaks at 1592.73 cm^{-1} and 1506.38 cm^{-1} indicate the presence of C=O in the quinone structure and deformation C=C of the aromatic rings of lignin respectively whereas peaks appearing at 1420.45 cm^{-1} 1317.74 cm^{-1}, and 1227.89 cm^{-1} are due to $^{-}$OH deformation, N-H stretching of the amine and C–O stretching of the phenolic group. Meanwhile the peak at 1030.27 indicate the presence of C-O and C-O-C due to ether group of cellulose while the peaks 517.94 and 431.92 could be due to $^{-}$OH out of plane bending modes [4, 9, 10, 22, 23].

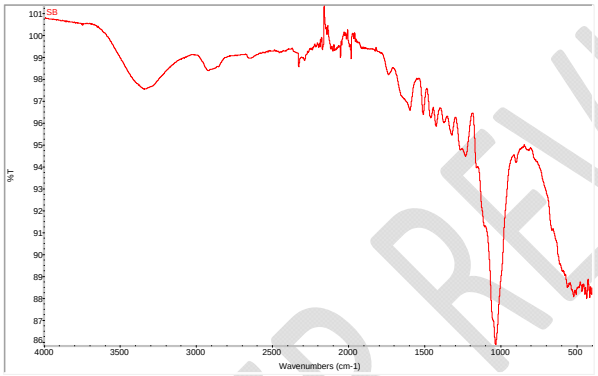

Fig. 2. Infrared spectra of sawdust

SEM images showing unmodified saw dust with different pore diameters and pore lengths are shown in Fig. 3 a and b. This indicate that unmodified saw dust is very porous with macropores with diameter greater than 1000 nm or 1 µm (Fig. 3 a and b) dominating. However, these pores have different lengths, longer in Fig. 3 than in Fig. 3a. Banerjee and Chattopadhyaya (2017) [10] also reported that saw dust is a heterogeneous material made up of irregular shapes with pores of varying sizes.

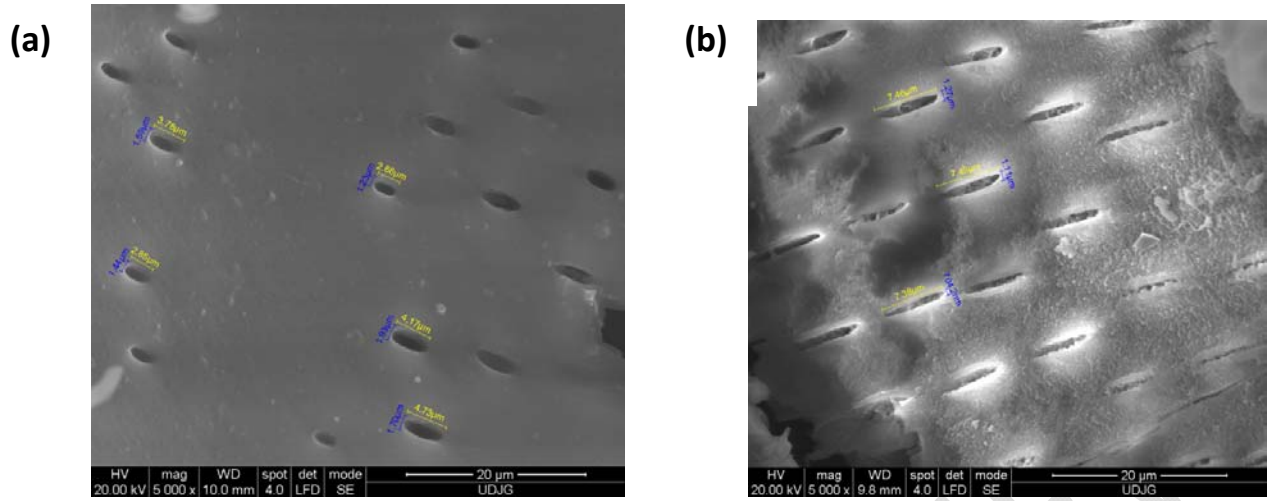

Fig. 3 SEM image of unmodified saw dust (a) shorter pores length, diameter < 2µm (b) longer pores length, some pores diameter >2µm.

1.2. Batch Adsorption Experiments

1.2.1. The effect of Contact Time and Initial Concentration

Fig. 4a presents the results of the effect of contact time for the removal of Cr(VI) using saw dust at three initial Cr(VI) concentrations. The adsorption of Cr(VI) is very rapid in the first two minutes, attaining more than 99 % for 50 and 100 mg/L initial concentrations and above 98 % for 10 mg/L. The rapidity of the adsorption is probably due to the availability of many ~~many~~ sites (as evident from FTIR and SEM analyses) on saw dust surface. Equally the pH and PZC of unmodified saw dust was found to be 8.29 and 2.2, consequently there were strong electrostatic attractions between the negative saw dust surface and the cationic Cr(VI) solution. However, for all the initial concentrations there is a slow down after the second minute in adsorption and attaining equilibrium in five minutes. This due to the reduction in the number of available active sites or the penetration of Cr(VI) ions in to the inner active sites of the adsorbent [24]. Higher adsorption at higher initial concentrations is due to the fact that there is an important driving force due to the increased concentration necessary to overcome all mass transfer resistances of the pollutant between the aqueous and solid phases thus increasing the adsorption.

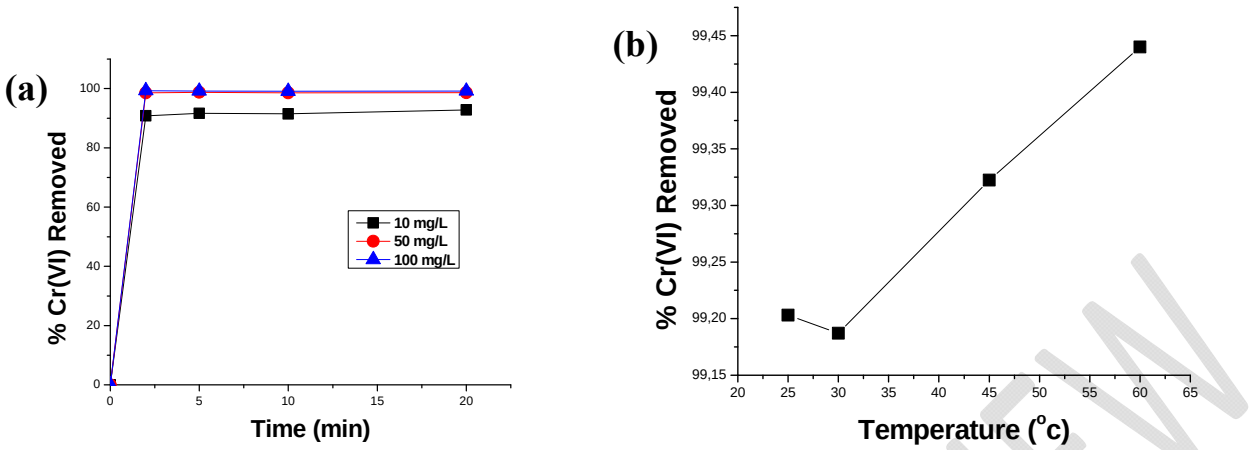

Fig. 4. Effects of (a) contact time (b) temperature on Cr(VI) adsorption by unmodified saw dust

1.2.2. The effect of Temperature

The results obtained are presented in Fig. 4b, where it is observed that increasing the temperature from 25-60 ^{o}C, increased the adsorption from 99.20 to 99.44 %. Although this shows an increase it is however marginal. The increase may be due to the creation of new active sites stemming from heating. This may also be attributed to the acceleration of some originally slow adsorption steps and enhancement of the mobility of adsorbate from the bulk solution towards the adsorbent surface [10].

1.3. Batch Adsorption Kinetics

Plots of the fitting of the different kinetic models are shown in Fig. 5 while the calculated kinetic parameters are presented in Table 1.

Pseudo-first-order model had a least fit to the equilibrium data, (Fig. 5a, Table 1) with very low R^2 values, increasing with increasing initial concentration. However, calculated q_e values did not match with the experimental values for all the three initial concentrations tested thus, indicating the unsuitability of this model.

The pseudo-second-order had a good fit, (Fig. 5b, Table 1) with all R^2 values at 100 % and a strong correlation between experimental and calculated q_e values. It is also observed from Table 1 that K_2 is highest for 50 mg/L showing fastest adsorption, however, h (initial adsorption rate) is highest for 100 mg/L (111111.11 for 100 mg/L against 100000 for 50 mg/L). This observation supports the fact

that higher adsorption at higher initial concentrations is due to the influence of an important driving force from increased concentration necessary to overcome all mass transfer resistances of the pollutant between the aqueous and solid phases thus increasing the adsorption.

The intraparticle diffusion model also presented less fitting to experimental data, Fig. 5c and Table 5. The intercept of the intraparticle diffusion model plot, Fig. 5c, reflects the boundary layer effect. The larger the intercept, the greater is the contribution of the surface sorption in the rate controlling step. Values of 18.01, 98.66 and 198.66 mg/g were obtained for 10, 50 and 100 mg initial concentrations. These values which are actually experimental q_e values indicate the existence of some boundary layer effect and further show that intraparticle diffusion was not the only rate-limiting step. For the process to be completely controlled by the intraparticle diffusion model, the plot should give a straight line passing through the origin. But the plots did not passed through the origin on at any initial concentration. This deviation from the origin is due to the difference in the rate of mass transfer in the initial and final stages of the sorption [25].

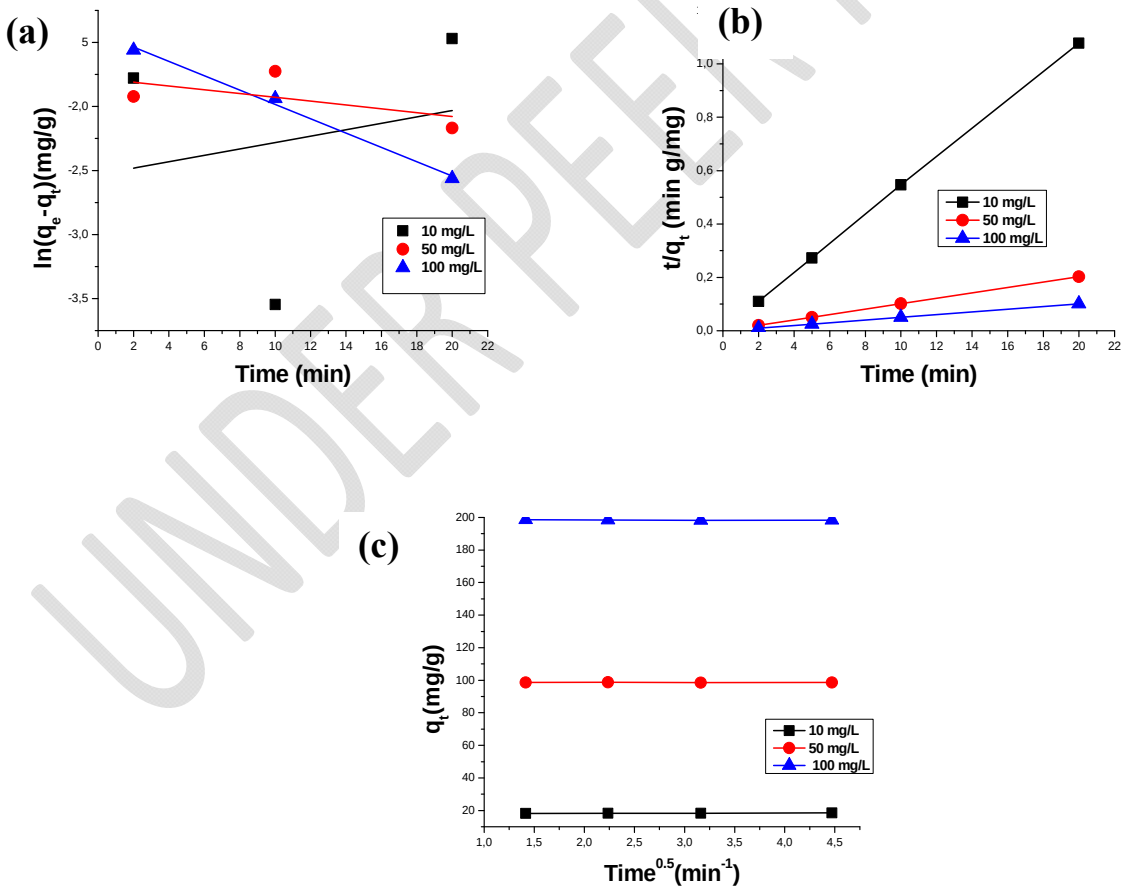

Fig. 5. (a) Pseudo-first order, (b) pseudo-second order and (c) intraparticle diffusion models kinetic plots for Cr(VI) removal on unmodified saw dust

Table 1. Kinetic parameters for Cr(VI) removal using saw dust

Models	Parameters	10 mg/L	50 mg/L	100 mg/L
Pseudo-first-order	k_1(min)	-0.025	0.015	0.056
	qe, cal (mg/g)	0.080	0.169	0.241
	*q*e, exp't (mg/g)	18.33	98.74	198.41
	R^2	0.041	0.367	0,994
Pseudo-second-order	k_2(g/mg/min)	0.627	10.20	2.78
	qe, cal (mg/g)	18.62	99.01	200.00
	qe, exp't (mg/g)	18.33	98.74	198.41
	R^2	1.000	1.000	1.000
	h(mg/g·min)	217.39	100000.00	111111.11
Intraparticle diffusion	k_{id} (mg/g/$min^{1/2}$)	0.117	0.009	0.090
	C (mg/g)	18.01	98.66	198.66
	qe, exp't (mg/g)	18.33	98.74	198.41
	R^2	0.8719	0.0216	0.604

qe, cal and *q*e, exp't are respectively, calculated and experimental equilibrium amounts adsorbed.

1.4. Batch Equilibrium Adsorption Isotherms

The equilibrium data was fitted to the linearized form of Langmuir isotherm model by plotting C_e/q_e versus C_e, Fig. 6a, and Langmuir parameters are presented in Table 2. It can be seen from this table that for all the concentrations studied, the coefficient of correlation was approximately unity. 14.87, 114.44 and 170.00 $Lmg^{-}1$ were the Langmuir equilibrium coefficient, b values obtained for the three initial concentrations used. These values were relatively high indicating favourable formation of

the saw dust Cr(VI) complex thus equilibrium is more shifted to the right or more Cr(VI) is adsorbed from solution by the saw dust. Furthermore, the Langmuir monolayer capacity, q_m, for all the tested initial concentrations were almost double the initial concentration used in each case, an indication that unmodified saw dust has a high adsorption capacity for hexavalent chromium.

The Freundlich isotherm model plot is shown in Fig. 6b and the determined parameters summarized in Table 2. Calculated R^2 values, Table 2 indicate that Freundlich isotherm represents a good fit to the equilibrium data for Cr(VI) adsorption on saw dust. Values of *n* in the range 2-10 represent good, 1-2 moderately difficult, and less than 1 a poor adsorptive potential [26]. However, the fact that $n > 10$ for all tested initial concentrations indicate that this model does not describe the adsorption of Cr(VI) adsorption on saw dust.

The Dubinin–Radushkevich (D–R) isotherm plot of $\ln q_e$ versus ε^2 is shown in Fig. 6c and its calcutated parameters presented in Table 2.While the Langmuir isotherm constants do not explain the chemical or physical properties of the adsorption process, mean adsorption energy (E) calculated from the D–R isotherm provides important information about these properties [27]. If the value of E is between 8 and 16 kJ/mol, ion exchange is the main sorption process in the system. If the value is lower than 8 kJ/mol, physical sorption is the main sorption mechanism and if the value is greater than 16 kJ/mol, it may be chemisorption [17, 28]. The Dubinin–Radushkevich constants were calculated and are shown in Table 2. For 10, 50 and 100 mg/L initial concentrations the corresponding values of E obtained were 5.59, 15.80 19.61 kJ/mol respectively for adsorption on unmodified saw dust. These results demonstrate that firstly adsorption on saw dust takes place by physical, ion exchange and chemisorption. Secondly, the mechanism of Cr(VI) adsorption on saw dust depends on its initial concentration. Thirdly, saw dust surface contain functional groups which under certain reaction conditions can form covalent bonds with Cr(VI). The good fit of the D-R isotherm, with all R^2 values greater than 0.99, suggests that adsorption on saw dust surface equally involves heterogeneous sites. The assumptions required by the Langmuir isotherm are less likely to be correct under industrial conditions because mixing of the adsorbent and the wastewater solution would be imperfect, thus the adsorbent surface is less likely to be homogeneous [28]. Thus, Dubinin–Radushkevich isotherm could be more appropriate for saw dust under industrial conditions due to the good fit.

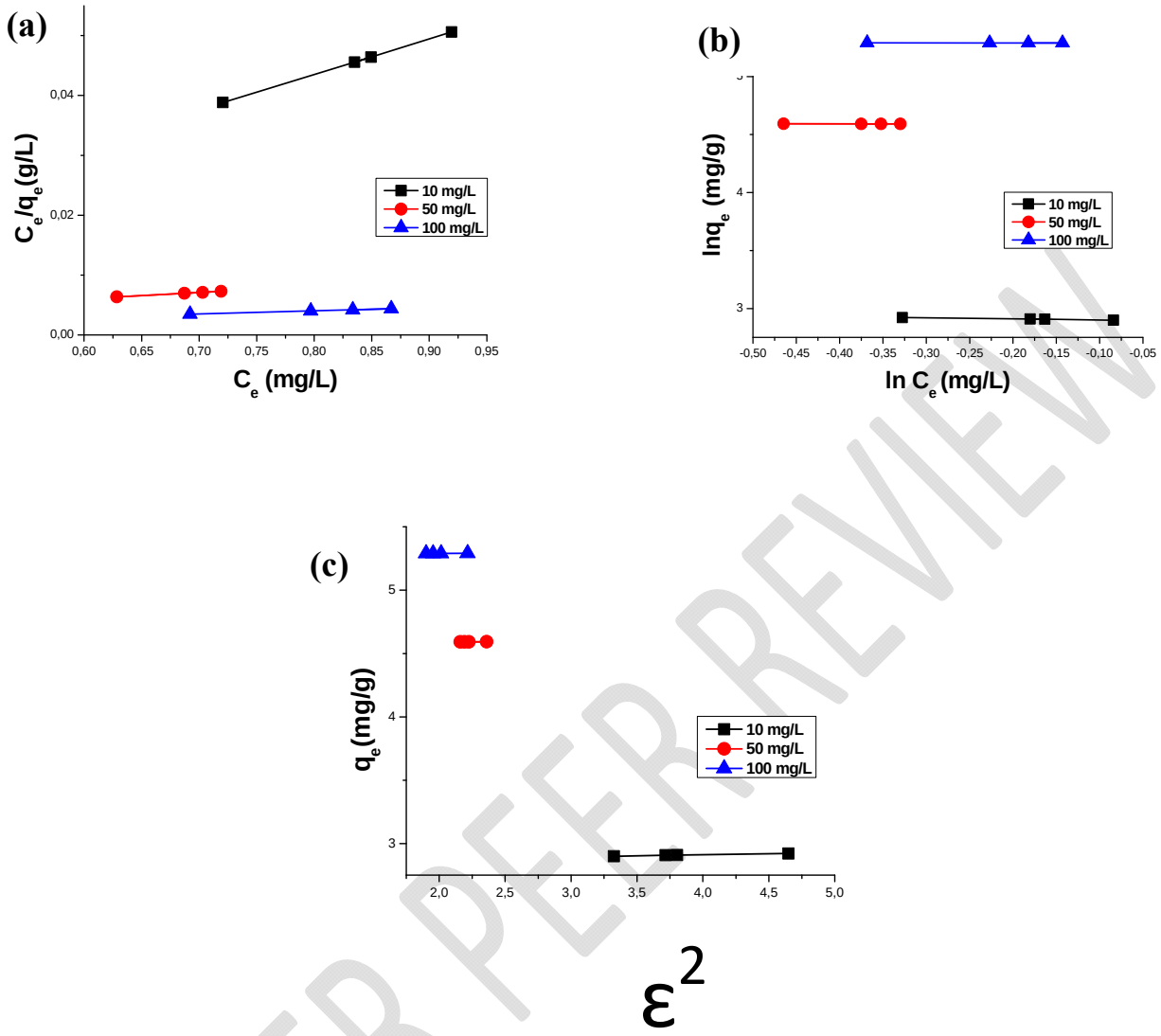

Fig. 6. (a) Langmuir, (b) Freundlich and (c) Dubinine Radushkevich isotherms plots for Cr(VI) removal on unmodified saw dust

Table 2. Isotherm parameters for Cr(VI) removal using saw dust

Models	Parameters	10 mg/L	50 mg/L	100 mg/L
Langmuir	q_m (mg/g)	84.03	97.08	196.08
	b (L/mg)	14.87	114.44	170.00
	R^2	0.9999	1.000	1.000
	R_L	0.0067	0.0002	0.0006
Freundlich	K_F (mg/g)(L/mg)$^{1/n}$	18.03	98.12	198.04
	n	11.34	73.53	128.20
	R^2	0.9982	0.9997	0.9991
Dubinin Radushkevich	Xm (mg/g)	17.23	97.74	197.31
	K (mol^2/KJ^2)	0.016	0.002	0.0013
	E (kJ/mol)	5.59	15.80	19.61
	R^2	0.9929	0.9989	0.9962

1.5. Batch Adsorption Thermodynamics

Table 3 presents the calculated thermodynamic parameters for Cr(VI) adsorption on unmodified saw dust. The obtained negative value for the Gibbs free energy shows that the adsorption process is spontaneous and that the degree of spontaneity of the reaction increases with increasing temperature. The overall adsorption process was endothermic (ΔH = 9.13 kJ mol^{-1}), suggesting that the adsorption capacity of saw dust increases with increasing temperature. Table 3 also shows that the ΔS value was positive. This shows the increased randomness at solid liquid interphase during the sorption processes. This according to [25] is a direct consequence of (i) opening up of structure of adsorbent beads (ii) enhancing the mobility and extent of penetration within the adsorbent beads and (iii) overcoming the activation energy barrier and enhancing the rate of intra-particle diffusion.

Table 3 Thermodynamic parameters for Cr(VI) removal by saw dust

C_0 (mg/L)	Temperature (K)	Equilibrium constant	ΔG° (KJ/mol)	ΔH° (KJ/mol)	ΔS° (KJ/mol K)	R^2
	298	124.48	-11.95			
C_0 = 100	303	122.02	-12.10	9.13	0.070	0.9589
	313	146.56	-12.98			
	333	167.56	-14.34			

C_0 = initial Cr(VI) concentration

1.6. Column Adsorption Experiments

1.6.1 Effect of Bed Height

The accumulation of adsorbate in the fixed-bed column is greatly depended on the quantity of adsorbent inside the column [20]. The breakthrough plot of the effect of bed height investigated at constant Cr(VI) concentration of 10 mg/L and flow rate of 17.28 mL/min is shown in Fig. 7a and calculated column parameters presented in Table 4. From Fig. 7a, it is observed that the slopes of the breakthrough curves decreases with increase bed height resulting in a broadened mass transfer zone. Equally, there is an increase in breakthrough time as bed height increased from 3.5-7 cm (7 minutes for 3.5 cm and15 minutes for 7 and 10 cm). The removal efficiency (Table 4), adsorption capacity, q_{total} (Table 4), and the saturation time (Fig. 7a) increased with increased in bed height. This result from the fact that Cr(VI) ions do not have sufficient time at low bed height to diffuse into the surface of the adsorbent causing a reduction in breakthrough time. Meanwhile increase in bed height, does not only lead to increase in surface area of adsorbent with more binding sites but also there is an increase in residence time of Cr(VI) solution inside the column thus permitting more diffusion of the Cr(VI) ions into the interior of the adsorbent hence more adsorption [21, 24].

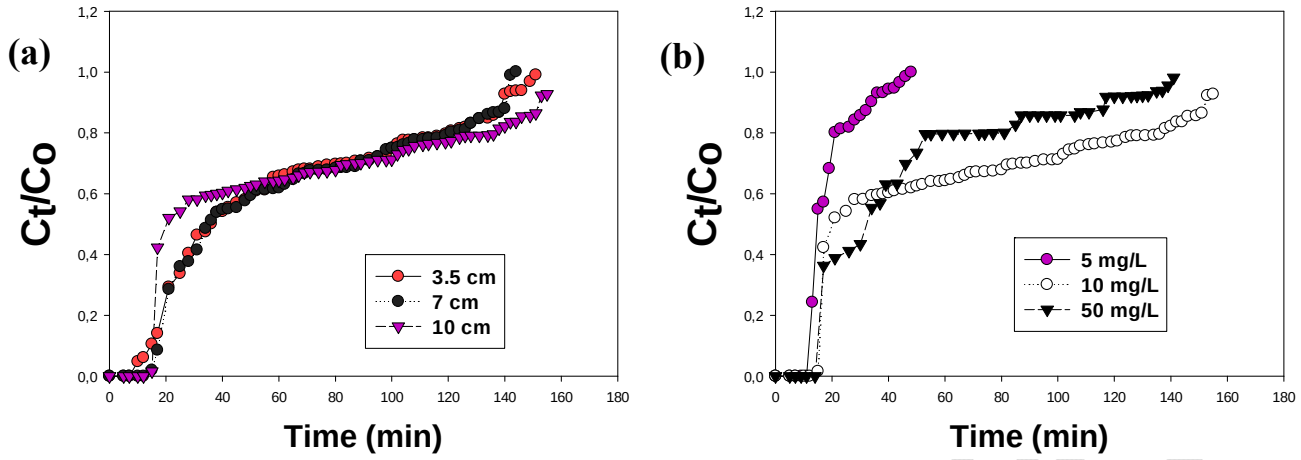

Fig. 7. Effect of (a) bed height (b) initial concentration on breakthrough curve for column removal of Cr(VI) by unmodified saw dust

Table 4 Column parameters of saw dust for Cr(VI) adsorption at different initial concentrations and bed heights

	V_{eff} (mL)	t_{total} (min)	q_{total} (mg)	q_{exp} (mg/g)	M_{total} (mg)	% Removal
Bed height						
3.5 cm	2609.28	151	10.13	2,23	26.09	38.83
7.0 cm	2488.32	144	10.32	1.00	24.88	41.48
10.0 cm	2678.40	155	10.02	0,66	26.78	37.42
Initial concentration						
5 mg/L	1309.44	48	1.63	0,16	4.15	39.28
10 mg/L	2678.40	155	10.02	0,97	26.78	37.42
50 mg/L	2436.48	141	39.06	3,78	121.82	32.06

1.6.2. Effect of Initial Concentration

Fig. 7b shows the effect of initial Cr(VI) concentration (5, 10 and 50 mg/L) studied at constant bed height of 10 cm and flow rate of 17.28 mL/min while the calculated column parameters are shown in Table 4. Contrary to other studies [20, 21, 24], the saturation time (Fig. 7b) and breakthrough time (11

minutes for 5 mg/L, 12 minutes for 10 mg/L and 14 minutes for 50 mg/L) increased with increase in initial concentration. However, the removal efficiency decreased with the increase in initial concentration (Table 4). These trends may probably due to the composition of saw dust that possibly led to the early creation of more binding sites as the saw dust used was from a mixture of different woods which quickly got saturated with increases in initial concentration. The adsorption capacity increased with increase in initial concentration increasing from 1.63 for 5 mg to 10.02 and 39.06 mg for 10 and 50 mg/L initial concentrations respectively (Table 4). There is a higher driving force at higher inlet concentration for the transfer process in order to overcome the mass transfer resistance [29].

1.6.3. Column Dynamic Adsorption Modeling

The Thomas Model

The column experimental data for the effect of initial concentration and bed height were fitted to the Thomas model as shown in Fig. 8 a and Fig. 8b respectively, while the calculated Thomas model parameter are given in Table 5. From the table, it there is a decrease in K_{Th} with increasing initial Cr(VI) inlet concentration but q_0 (mg/g) values were increasing. This is due to the driving force of adsorption for the difference in concentrations between Cr(VI) on the adsorbent surface and in the solution [30]. The K_{Th} rate constant and maximum sorption capacity q_0 all decreased with increasing bed height (Table 5). The increase in q_o with increase in bed height (which corresponds to increase in adsorbent mass) means more adsorption sites being available for Cr(VI) ions. The decrease in the rate constant of the Thomas model K_{Th}, indicates an increase in the mass transport resistance with increase bed height. Thomas model gave a more good fit of the experimental data for the effect of initial concentration with maximum R^2 value of 92 % compared the effect of bed height with maximum R^2 value of 80 % (Table 5). This shows that Thomas model was suitable for adsorption processes where external and interior diffusions were not the rate limiting steps [21, 31].

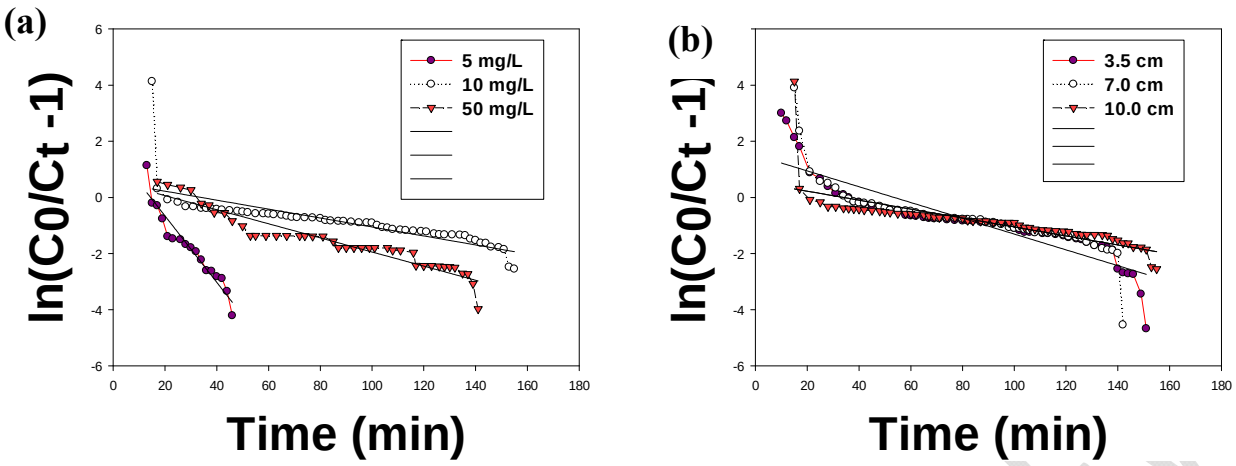

Fig. 8. Thomas kinetic plots for the adsorption of Cr(VI) on saw dust at different (a) initial concentration and (b) bed height

The Yoon-Nelson Model

A plot of the Yoon-Nelson model for the effect of initial concentration and effect of bed height are shown in Fig. 9 a and b while the evaluated parameters are presented in Table 5. In comparison to Thomas model, R^2 values obtained were very low with a maximum of 60 and 65 % for the effect of initial concentration and bed height respectively. From table 5 it can be seen that as the initial concentration increased at constant flow rate K_{YN} decreased while τ (time required for retaining 50 %) increased. This likely due to low diffusion to the adsorbent surface at higher concentration with a constant flow rate as the Cr(VI)residence time increases in the column. There was a significant simultaneous decrease in the rate constant and τ as bed height increased at constant flow rate. This is due to the mass transfer resistance in the column due to use of constant flow rate used which do not facilitate easy distribution of the ions on the adsorbent surface in the column.

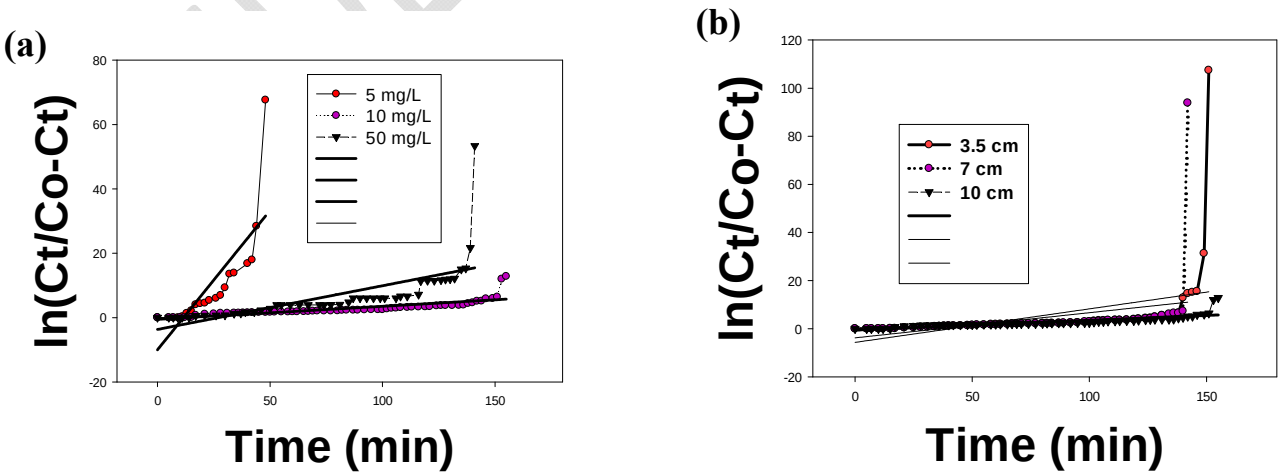

Fig. 9. Young-Nelson kinetic plots for the adsorption of Cr(VI) on saw dust at different (a) initial concentration and (b) bed height

Table 5. Modelling of column kinetic parameters for the removal of Cr(VI) using Thomas and Yoon - Nelson Models

	Thomas model			Yoon-Nelson model		
Initial concentration (mg/L)	K_{TH}(mL/min/mg)	q_o (mg/g)	R^2	K_{YN}(min^{-1})	τ	R^2
5	0.024	81.57	0.921	0.867	0.087	0.603
10	0.002	311.77	0.586	0.040	12.847	0.657
50	0.001	651.07	0.904	0.136	27.018	0.481
Bed height (cm)						
3.5	0.003	1914.88	0.804	0.139	40.685	0.187
7	0.003	747.18	0.697	0.421	53.378	0.031
10	0.002	311.77	0.586	0.041	13.617	0.650

4. CONCLUSION

The investigation of the use of unmodified saw dust, a low cost adsorbent for the removal of hexavalent chromium from aqueous solution in batch and column operations was undertaken in this study. In batch study, nearly 99 % Cr(VI) was removed in just two minutes at low and high concentrations tested with the process being very spontaneous and endothermic. While the Langmuir and D-R isotherms best fitted the batch equilibrium adsorption process, pseudo-second order kinetic model best described the kinetics of the process. Langmuir and D-R isotherms results show that homogenous and heterogeneous

sites are involved in the adsorption of Cr(VI) on saw dust surface. The influence of Cr(VI) initial concentration and bed height were used to investigate the column removal process. Increased in these two factors studied increased breakthrough times and adsorption capacities. Column experimental data fitted to Thomas and Yoon - Nelson kinetic models showed that Thomas model best fitted the column adsorption process with higher correlation coefficients showing that the external and internal diffusions were not the rate limiting steps. From the findings of this study, unmodified saw dust, a low cost and easily available saw mill waste can be used to treat wastewater containing hexavalent chromium.

REFERENCES

1. Singh N, Gupta SK. Adsorption of Heavy Metals: A Review. International Journal of Innovative Research in Science. Engineering and Technology. 2016;5(2):2267-2281.

2. Parvin S, Tasnim L, Mazumder, Hasan S, Rabbani KA, Rahman ML. What Should We Do With Our Solid Tannery Waste? IOSR Journal of Environmental Science, Toxicology and Food Technology (IOSR-JESTFT). 2017;11(4):82-89.

3. Nair ADG, Hansdah K, Dhal B, Mehta KD, Pandey BD. Bioremoval of Chromium (Iii) from Model Tanning Effluent by Novel Microbial Isolate. International Journal of Metallurgical Engineering. 2012;1(2):12-16.

4. Fatima B, Werdia B, Rabah BL, Ahmed B, Ama A, Khaled B, Naima B. Valorization of sawdust using Biological denirification of synthetic nitrates-contaminated ground water. Research Journal of Chemistry and Environment. 2018;22 (7):42-50.

5. Kimbrough DE, Cohen Y, Winer AM, Creelman L, Mabuni C. A Critical Assessment of Chromium in the Environment. Critical Reviews in Environmental Science and Technology. 1999: 29(1):1-46.

6. Bruce J. Analysis of chromium in waters using voltammetry. Metrohm UK, Laboratory talk. 2002.

7. Gebrekidan M, Samuel Z. Concentration of Heavy Metals in Drinking Water from Urban Areas of the Tigray Region, Northern Ethiopia. CNCS, Mekelle University ISSN: 2220-184X. 2011;3(1):105-121.

8. Tejada-Tovar C, Villabona-Ortíz A, Herrera-Barros A, González-Delgado AD, Garcés L. Adsorption Kinetics of Cr (VI) using Modified Residual Biomass in Batch and Continuous System. Indian Journal of Science and Technology. 2018;11(4) 1-8.

9. Bello OS, Adelaide OM, Hammed MA, Popoola OAM. Kinetic and equilibrium studies of methylene blue removal from aqueous solution by adsorption on treated sawdust. Macedonian Journal of Chemistry and Chemical Engineering 2010;29(1):77–85.

10. Banerjee S, Chattopadhyaya MC. Adsorption characteristics for the removal of a toxic dye, tartrazine from aqueous solutions by a low cost agricultural by-product. Arabian Journal of Chemistry. 2017;10(2):S1629-S1638.

11. Boumaza S, Yenounne A, Hachi W, Kaouah F, Bouhamidi Y, Trari M. Application of Typha angustifolia (L.) Dead Leaves Waste as Biomaterial for the Removal of Cationic Dye from Aqueous Solution. International Journal of Environmental Research. 2018;12:561–573.

12. El-Nahas S, Salman HMA, Seleem WAM. A New and Successful Utilization of Egypt alum Company Solid Waste in Adsorptive Removal of Nitrates from Water Supplies. International Research Journal of Pure & Applied Chemistry. 2017;15(3):1-17.

13. Rodier J, Legube B, Merlet N et coll. L'Analyse de l'eau. 9^{e} édition Dunod, Paris France. 2009;1579 pages.

14. Jeyakumar RPS, Chandrasekaran V. Adsorption of lead (II) ions by activated carbons prepared from marine green algae: equilibrium and kinetics studies. International Journal of Industrial Chemistry. 2014; 5:10.

15. Tsamo C, Tchouanyo DJH, Meali DS. Treatment of Red Mud with Distilled Water to Improve Its Efficiency to Remove Methylene Blue from Aqueous Solution. International Research Journal of Pure & Applied Chemistry. 2017;15(3):1-19.

16. Saravanan D, Sudha PN. Batch Adsorption Studies for the Removal of Copper from Wastewater using Natural Biopolymer. International Journal of ChemTech Research. 2014;6(7):3496-3508 .

17. Saranya N, Nakkeeran E, Shrihari S, Selvaraju N. Equilibrium and Kinetic Studies of Hexavalent Chromium Removal Using A Novel Biosorbent: Ruellia Patula Jacq. Arabian Journal for Science and Engineering. 2017; 42(4):1545–1557.

18. Oyelude EO, Awudza JAM, Twumas S K. Removal of malachite green from aqueous solution using pulverized teak leaf litter: equilibrium, kinetic and thermodynamic studies. Chemistry Central Journal. 2018;12: 81.

19. Guo J, Lua AC. Textural and chemical properties of adsorbent prepared from palm shell by phosphoric acid activation. Material Chemistry and Physics. 2003;80:114-9.

20. Attia AAM, Shouman MAH, Khedr SAA, Hassan NA. Fixed-Bed Column Studies for the Removal of Congo Red Using *Simmondsia chinesis* (Jojoba) and Coated with Chitosan. Indonesian Journal of Chemistry. 2018;18(2):294 – 305.

21. Alamin AH, Kaewsichan L. Adsorption of Pb(II) Ions from Aqueous Solution in Fixed Bed Column by Mixture of Clay plus Bamboo Biochar. Walailak Journal of Science and Technology. 2016;13(11):949-963.

22. Tsa WT, Chang CY, Lin MC, Chien SF, Sun HF, Hsieh MF. Adsorption of acid dye onto activated carbon prepared from agricultural waste by $ZnCl_2$ activation. Chemosphere. 2001;45(1):51-58.

23. Azlina W, Wan AB, Ghani K. Saw-dust Biochar: Characterization and CO_2 adsorption/desorption study. Journal of Applied Sciences. 2014;14:1450-1454.

24. Mobasherpour I, Salahi E, Asjodi A. Research on the Batch and Fixed-Bed Column Performance of Red Mud Adsorbents for Lead Removal. Canadian Chemical Transactions. 2014;2(1):83-96.

25. Murugan SO, Arivoli S. Equilibrium, Kinetic and Thermodynamic Study on Malachite Green dye Removal from Aqueous Solution using Activated Los Pantanos De Villa Nano Carbon. IJRDO-Journal of Applied Science. 2017;3(1):Paper-3

26. **Shikuku VO, Chrispin O. Kowenje CO, Kengara FO.** Errors in Parameters Estimation Using Linearized Adsorption Isotherms: Sulfadimethoxine Adsorption onto Kaolinite Clay. Chemical Science International Journal. 2018;23(4):1-6.

27. Argun ME, Dursun S, Ozdemir C, Karatas M. Heavy metal adsorption by modified oak sawdust: Thermodynamics and kinetics. Journal of Hazardous Materials. 2007;141:77–85.

28. Alfaro-Cuevas-Villanueva R, Hidalgo-Vázquez AR, Penagos CC, Cortés-Martínez R. Thermodynamic, Kinetic, and Equilibrium Parameters for the Removal of Lead and Cadmium from Aqueous Solutions with Calcium Alginate Beads. The Scientific World Journal. 2014;2014:10 pages.

29. Lakshmipathy R, Sarada NC. A fixed bed column study for the removal of Pb^{2+} ions by watermelon rind. Environmental Science: Water Research & Technology. 2015;1(2):244-50.

30. Lin X, Li R, Wen Q, Wu J, Fan J. Jin X, Qian W, Liu D, Chen X, Chen Y, Xie J, Bai J, Ying H. Experimental and modeling studies on the sorption breakthrough behaviors of butanol from aqueous solution in a fixed-bed of KA-I resin. Biotechnology and Bioprocess Engineering. 2031;18(2):223–233.

31. Albadarin AB, Mangwandi C, Al-Muhtaseb AH, Walker GM, Allen SJ, MNM Ahmad MNM. Modelling and fixed bed column adsorption of Cr(VI) onto orthophosphoric acid-activated lignin. Chinese Journal of Chemical Engineering. 2012;20(3):469-77.